Analytical Modeling of Magnetic Field Considering the Saturation in Switched Reluctance Motor

Shenglong Hu and Shuguang Zuo*

Clean Energy Automotive Engineering Center
Tongji University, Shanghai, 201804, China
slhu825@163.com, sgzuo@tongji.edu.cn*

Abstract ─ This paper aims at accurately predicting the severe magnetic saturation of a switched reluctance motor (SRM). Firstly, Method I based on the solution of the Laplacian or Poissonian field equation is used to predict the magnetic field in the air gap, but this method is only applicable to the mildly saturated magnetic field. Secondly, Method II based on the winding function theory (WFT) considering the saturation is utilized to predict the magnetic field, which can precisely compute the severely saturated magnetic field. Nevertheless, the tangential magnetic flux density is not considered by Method II. Finally, the synthetic method based on the advantages of Method I and Method II is proposed, which can predict the air-gap magnetic field in SRM having any number of stator slots and rotor poles for any rotor positions. The results indicate that the error of the air-gap magnetic field obtained by the synthetic method is within 5%. Moreover, the radial electromagnetic force and torque obtained by the Maxwell Stress equation are compared with the results computed by the FEM, verifying the effectiveness of the synthetic method. It lays the groundwork for the optimization of torque ripple, vibration and noise of SRM.

Index Terms ─ Analytical modeling, magnetic field, saturation and switched reluctance motor.

I. INTRODUCTION

In recent years, SRMs are widely used in the aerospace, high-speed centrifugal compressor, electric vehicle, mine and so on due to its strong robustness, simple structure, high temperature resistance and low cost [1-3]. Nevertheless, SRM compared with other motors has a much larger torque ripple, vibration and noise, which limits its broader application [4-6]. Therefore, it is necessary to establish an analytical model that can accurately reflect the parameters of motor, which lays the foundation for the optimization of torque ripple, vibration and noise.

At present, there is much literature on the analytical modeling of the motor magnetic field, which mainly includes the analytical method based on the solution of the Laplacian or Poissonian field equation and the other analytical method based on WFT. In [7-9], the method based on the solution of the Laplacian or Poissonian field equation has been applied to predict the air-gap magnetic field of surface mounted permanent magnetic brushless DC motors. In [10-12], the magnetic field distribution of flux-switching machine, surface mounted permanent-magnet synchronous motor and disc-type permanent generator was also predicted respectively through the above analytical method. In [13], the analytical modeling based on the solution of the Laplacian or Poissonian field equation considering the magnetic saturation has also been implemented, which was a semi-analytical method depending on the results of FEM. In [14], the method based on the solution of Laplacian or Poissonian field equation has been also applied and an iterative algorithm of saturation according to the working principle of induction motor has been proposed, however, the iterative algorithm about saturation was not applicable for SRM on account of the particular working principle. In [15], the above analytical method has been utilized to predict the magnetic field distribution in SRM and the magnetic saturation was also considered. However, it was not appropriate for the severe magnetic saturation but the mild magnetic saturation.

There are also lots of references on analytical modeling based on WFT. In [16-18], the air-gap magnetic field of interior permanent magnetic (IPM) motor has been predicted by the analytical method based on WFT, but the magnetic saturation was not taken into account. In [19], the magnetic field distribution of flux-switching machine has been computed with the above analytical method. However, the saturation problem has also been neglected. In [20], the magnetic field distribution considering the saturation of rotor in fractional-slot concentrated-wound IPM motor has been computed with the analytical method based on WFT. Nevertheless, the method based on WFT in the above literature only predicts the radial magnetic flux density, neglecting the tangential magnetic flux density. However, the slot width of SRM is larger than that of other motors, which results in severe magnetic flux leakage at the tooth

Submitted On: May 21, 2018
Accepted On: October 19, 2018

backlash, so that the magnetic flux density has a larger tangential component. Therefore, the tangential magnetic flux density cannot be ignored.

From the above, there is little literature about the analytical modeling of air-gap magnetic field considering the saturation in SRM. Moreover, the analytical modeling of magnetic saturation results from the doubly salient structure has been difficult. This paper aims at accurately predicting the severe magnetic saturation of SRM with the analytical method.

The originality in this paper includes two main points. Firstly, based on the idea of the distributed equivalent circuit with the series reluctance, a new algorithm of magnetic saturation is proposed, which combines the specific relationship between the permeability and the magnetic flux density of the iron core material. Secondly, the synthetic analytical method of the air-gap magnetic field of SRM based on the solution of the Laplacian or Poissonian field equation and WFT is presented, which can be applied to predict the air-gap magnetic field in SRM having any number of stator slots and rotor poles for any rotor positions.

II. THE MAIN PARAMETERS OF SRM

The proposed motor is a three-phase 6/4 SRM. Moreover, the main parameters are shown in Table 1.

Table 1: Main parameters of three-phase 6/4 SRM

Parameter	Symbol	Value
Number of stator poles	N_s	6
Number of rotor poles	N_r	4
Number of slot coil	N_c	66
Width of stator slot	θ_{ss}	0.524 rad
Width of one slot coil	d	0.154 rad
Air gap length	g	4 mm
Internal radius of stator	R_s	41.4 mm
External radius of rotor	R_r	41.0 mm
Internal radius of rotor slot	R_1	30.0 mm
External radius of stator slot	R_4	62.5 mm
Length of stator pole	h_s	21.1 mm
Length of rotor pole	h_r	11 mm
Length of rotor core	h	91.5 mm

III. METHOD I

Method I is used to predict the air-gap magnetic field of SRM by solving the Laplacian or Poissonian field equation. In [15], although the magnetic field of SRM was computed with Method I, the solution of the inverse matrix was unstable and difficult due to the large matrix dimension. Based on the analytical model in [15], Method I makes the following modifications to the column vector consisting of the coefficients of current density, the convolution matrixes of radial and tangential magnetic permeability.

According to [15], the complex Fourier series expansion of current density in the three-phase 6/4 SRM in Fig. 1 is shown in Eq. (1):

$$J(\theta)=\sum_{n=-\infty}^{\infty}J_n e^{-jn\theta}, \tag{1}$$

The coefficients of J_n are computed as;

$$J_n=\sum_{i=1}^{N_s}\frac{1}{2\pi jn}\begin{bmatrix}J_{1,i}e^{-jn\theta_{ss}/2}\left(e^{jnd}-1\right)+\\ J_{2,i}e^{jn\theta_{ss}/2}\left(1-e^{-jnd}\right)\end{bmatrix}e^{jn\alpha_i}. \tag{2}$$

In Eq. (2), θ_{ss} is the slot width, d is the width of a single slot coil, the values $J_{1,I}$,$J_{2,I}$,α_i are defined as follows:

$$J_{1,i}=N_c/S\cdot\begin{bmatrix}-i_a & i_b & -i_c & i_a & -i_b & i_c\end{bmatrix}^T, \tag{3}$$

$$J_{2,i}=N_c/S\cdot\begin{bmatrix}-i_b & i_c & -i_a & i_b & -i_c & i_a\end{bmatrix}^T, \tag{4}$$

$$\alpha_i=2\pi/N_s\cdot i-\pi/N_s. \tag{5}$$

In Eqs. (3) and (4), S is the area of the stator slot coil. $\mathbf{J_z}$ is the column vector composed of the coefficients J_n, which is presented in Eq. (6). To acquire the inverse matrix more efficiently, the modified column vector of the coefficients of current density does not include J_0 because the DC component J_0 is equal to zero:

$$\mathbf{J_z}=\begin{bmatrix}J_{-N} & \cdots & J_{-1} & , & J_1 & \cdots & J_N\end{bmatrix}^T. \tag{6}$$

In the same way, the complex Fourier series expansion of magnetic permeability can be obtained and the coefficients of radial magnetic permeability can compose one matrix $\boldsymbol{\mu_r}$. To make the dimension of $\boldsymbol{\mu_r}$ are consistent with that of $\mathbf{J_z}$, the matrix $\boldsymbol{\mu_r}$ needs to be revised, as shown in Eq. (7):

$$\boldsymbol{\mu_r}=\begin{bmatrix}\mu_0 & \cdots & \mu_{-n+1} & \mu_{-n-1} & \cdots & \mu_{-2n}\\ \vdots & \ddots & \vdots & \vdots & \ddots & \vdots\\ \mu_{n-1} & \cdots & \mu_0 & \mu_{-2} & \cdots & \mu_{-n-1}\\ \mu_{n+1} & \cdots & \mu_2 & \mu_0 & \cdots & \mu_{-n+1}\\ \vdots & \ddots & \vdots & \vdots & \ddots & \vdots\\ \mu_{2n} & \cdots & \mu_{n+1} & \mu_{n-1} & \cdots & \mu_0\end{bmatrix}. \tag{7}$$

Based on the matrix $\boldsymbol{\mu_r}$, the modified matrix $\boldsymbol{\mu_t}$ consisting of the coefficients of tangential magnetic permeability can be calculated, as shown in Eq. (8), where μ^{rec} can be obtained by replacing μ in the complex Fourier series expansion of radial magnetic permeability with $1/\mu$:

$$\boldsymbol{\mu_t}=\begin{bmatrix}\mu_0^{rec} & \cdots & \mu_{-n+1}^{rec} & \mu_{-n-1}^{rec} & \cdots & \mu_{-2n}^{rec}\\ \vdots & \ddots & \vdots & \vdots & \ddots & \vdots\\ \mu_{n-1}^{rec} & \cdots & \mu_0^{rec} & \mu_{-2}^{rec} & \cdots & \mu_{-n-1}^{rec}\\ \mu_{n+1}^{rec} & \cdots & \mu_2^{rec} & \mu_0^{rec} & \cdots & \mu_{-n+1}^{rec}\\ \vdots & \ddots & \vdots & \vdots & \ddots & \vdots\\ \mu_{2n}^{rec} & \cdots & \mu_{n+1}^{rec} & \mu_{n-1}^{rec} & \cdots & \mu_0^{rec}\end{bmatrix}^{-1}. \tag{8}$$

According to the above analysis, the modified column vector $\mathbf{J_z}$, the convolution matrixes $\boldsymbol{\mu_r}$ and $\boldsymbol{\mu_t}$ can be captured. In the following, the air-gap magnetic field distribution will be computed based on the above

analysis. The air-gap magnetic field is determined by the magnetic field in the stator and rotor slots/teeth region due to the particular doubly salient structure of SRM, so the magnetic field in the stator and rotor slots/teeth region should be taken into account. According to [15], the magnetic vector potential in the air gap region and the stator slots/teeth region and the rotor slots/teeth region can be solved by corresponding Laplacian or Poissonian field equation.

The magnetic field calculated by the above method is linear. However, regional saturation is severe on account of the doubly salient structure and the particular working principle of SRM, especially the stator/rotor poles under excitation state. Therefore, the magnetic saturation of SRM must be taken into account. According to the iterative algorithm of magnetic saturation in [15], the air-gap magnetic flux density can be obtained, which is based on the accurate magnetic flux density in the stator and rotor slots/teeth region. Moreover, the magnetic flux densities in the air gap considering the saturation of three-phase 6/4 SRM at the unaligned and aligned position are shown in Fig. 1 and Fig. 2, respectively, which are calculated by Method I.

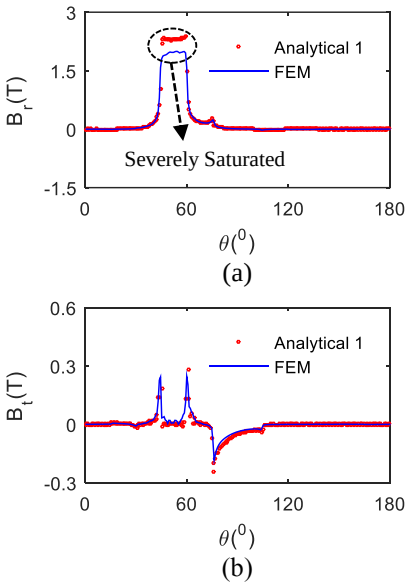

Fig. 1. The magnetic flux density at the unaligned position: (a) radial and (b) tangential.

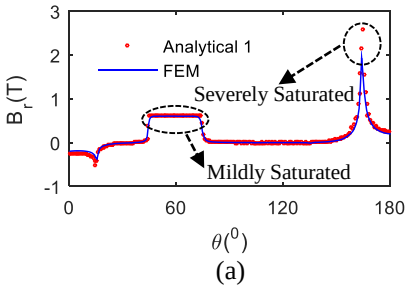

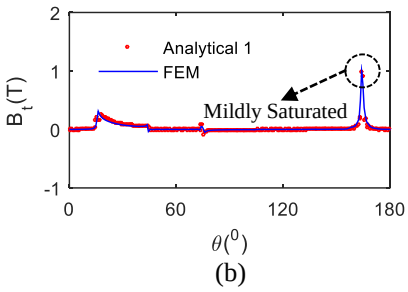

Fig. 2. The magnetic flux density at the aligned position: (a) radial and (b) tangential.

It can be observed in Fig. 1 and Fig. 2 that the magnetic flux density obtained by Method I is in good agreement with the result of FEM in the mildly saturated region. However, in the severely saturated region, especially in the stator/rotor poles under the excitation state, the error of Method I and FEM is significant and the maximum error is more than 20%. Besides, the tangential magnetic flux density obtained by Method I has a nice agreement with the FEM, but the radial magnetic flux density is not accurate. Because the tangential magnetic flux density is mildly saturated and the radial magnetic flux density is severely saturated. In addition, the iterative algorithm of air-gap magnetic saturation is based on the accurate magnetic flux density in the stator and rotor slots/teeth region. However, it is difficult to accurately calculate the magnetic flux densities in the stator and rotor slots/teeth region for severe magnetic saturation, so that the error of the air-gap magnetic field in the severely saturated region is enormous. Although the analytical magnetic field in [15] was in good agreement with the FEM, the selected motor worked under the mildly saturated condition, in which the maximum magnetic flux density is below 1.5 T. However, the magnetic saturation of SRM in this paper is severe and the maximum magnetic flux density is over 2 T, so the iterative algorithm considering the saturation is no longer working. In view of the knotty problem of magnetic saturation, this paper presents another analytical method, namely Method II, which will be introduced detailedly in the following.

IV. METHOD II

Method II is a kind of analytical modeling based on WFT and the specific modeling thinking is as follows.

A. The radial magnetic flux density without slot opening

The spatial distribution of magnetomotive force (MMF) of the qth-phase winding in SRM is shown in Fig. 3. Where $\alpha=N_r\theta$, N_c is the number of coil turns in one tooth, i_q the qth-phase current, β_s is the width of stator tooth, N_r is the number of rotor poles, N_t is the

number of stator pole pairs, $N_t=N_s/(2Q)$, Q is the number of phases and $1\le q\le Q$.

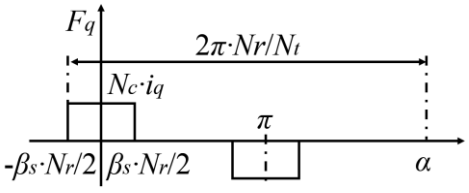

Fig. 3. The spatial distribution of MMF.

So, the Fourier series expansion of the qth-phase winding is given by Eq. (9) [16-18]:

$$F_q(\theta)=\sum_{v=1,3,5}^{\infty}F_v\cos(vN_t\theta). \tag{9}$$

The value of F_v is calculated though Eq. (10):

$$F_v=4N_c i_q/(\pi v)\cdot\sin(N_t\beta_s v/2). \tag{10}$$

Then, the Fourier series expansion of the qth-phase current is shown as:

$$i_q(t)=\sum_{i=0}^{\infty}I_i\cos(iN_r\omega t). \tag{11}$$

The value of I_i in Eq. (11) is given as follows, where θ_c is the conduction angle:

$$I_i=\begin{cases}I_0\theta_c N_r/(2\pi), & i=0\\ 2I_0/(\pi i)\cdot\sin(\theta_c N_r i/2), & i=1,2\cdots.\end{cases} \tag{12}$$

Equation (11) is substituted to Eq. (10); then, Eq. (10) is substituted to Eq. (9). Then, the Fourier series expansion of MMF of the qth-phase winding can be obtained, as shown in Eq. (13). Where v=1,3,5…, i=0,1,2…, K_{vi} is the coefficient associated with v, i:

$$F_q(\theta,t)=\sum_{v}^{\infty}\sum_{i}^{\infty}K_{vi}\cos(vN_t\theta\pm i\omega N_r t). \tag{13}$$

Assume $u=vN_t$; the Eq. (13) can be written as Eq. (14), where K_{ui} is the coefficient associated with u, i:

$$F_q(\theta,t)=\sum_{u}^{\infty}\sum_{i}^{\infty}K_{ui}\cos(u\theta\pm i\omega N_r t). \tag{14}$$

Based on the working principle of SRM, the MMF of different phase winding can be written as Eq. (15), where N_s is the number of stator poles:

$$\begin{cases}F_1=\sum_{u}^{\infty}\sum_{i}^{\infty}K_{ui}\cos(u\theta\pm i\omega N_r t)\\ F_2=\sum_{u}^{\infty}\sum_{i}^{\infty}K_{ui}\cos\left[u\left(\theta+\frac{2\pi}{N_s}\right)\pm i\omega N_r\left(t-\frac{2\pi}{q\omega N_r}\right)\right]\\ F_3=\sum_{u}^{\infty}\sum_{i}^{\infty}K_{ui}\cos\left[u\left(\theta+\frac{4\pi}{N_s}\right)\pm i\omega N_r\left(t-\frac{4\pi}{q\omega N_r}\right)\right]\end{cases}. \tag{15}$$

According to the literature [19], the radial magnetic flux density of the qth-phase winding without slot opening can be given by Eq. (16), which is written as Eq. (17), where μ_0 is the air permeability, g is the length of the air gap:

$$B_{rq0}(\theta,t)=F_q(\theta,t)\cdot\Lambda_0, \tag{16}$$

$$B_{rq0}(\theta,t)=\frac{\mu_0}{g}\sum_{u}^{\infty}\sum_{i}^{\infty}K_{ui}\cos(u\theta\pm iN_r\omega t). \tag{17}$$

B. The influence of slot opening in stator and rotor

Suppose the coefficient of stator pole is 1 and the influence coefficient of the stator slot is ε_s.

Besides, the Fourier series expansion of the influence coefficient of the stator slot is given in Eq. (18) [18]:

$$\lambda_s(\theta)=\lambda_{s0}+\sum_{m=1}^{\infty}\lambda_{sm}\cos(mN_s\theta), \tag{18}$$

where the values of λ_{s0} and λ_{sm} are shown as follows:

$$\lambda_{s0}=\varepsilon_s+(1-\varepsilon_s)\beta_s N_s/(2\pi), \tag{19}$$

$$\lambda_{sm}=2/(\pi m)\cdot(1-\varepsilon_s)\sin(\beta_s N_s m/2). \tag{20}$$

The analysis of the influence coefficient of the rotor slot is the same as stator slot. Suppose the coefficient of the rotor pole is 1 and the influence coefficient of the rotor slot is ε_r. The Fourier series expansion of the influence coefficient of the rotor slot is given in Eq. (21) [18]:

$$\lambda_r(\theta,t)=\lambda_{r0}+\sum_{n=1}^{\infty}\lambda_{rn}\cos(nN_r\theta-n\omega N_r t), \tag{21}$$

Moreover, the values of λ_{r0} and λ_{rn} are shown as follows:

$$\lambda_{r0}=\varepsilon_r+1/(2\pi)\cdot(1-\varepsilon_r)\beta_r N_r, \tag{22}$$

$$\lambda_{rn}=2/(\pi n)\cdot(1-\varepsilon_r)\sin(\beta_r N_r n/2). \tag{23}$$

Furthermore, the product of the influence coefficient of stator and rotor slot is given in Eq. (24):

$$\begin{aligned}\lambda_{sr}(\theta,t)&=\lambda_s(\theta)\times\lambda_r(\theta,t)\\ &=\lambda_{s0}\lambda_{r0}+\sum_{m=1}^{\infty}\lambda_{r0}\lambda_{sm}\cos(mN_s\theta)+\\ &\sum_{n}^{\infty}\lambda_{s0}\lambda_{rn}\cos(nN_r\theta-n\omega N_r t)+\\ &\sum_{m}^{\infty}\sum_{n}^{\infty}\frac{1}{2}\lambda_{sm}\lambda_{rn}\cos\left[(mN_s\pm nN_r)\theta\mp n\omega N_r t\right].\end{aligned} \tag{24}$$

C. The radial magnetic flux density with slot opening

Through the above analysis, the radial magnetic flux density of the qth-phase winding without slot opening, the influence coefficient of stator and rotor slot has been gotten, respectively. According to [16-18], the radial magnetic flux density of the qth-phase winding with slot opening can be obtained, which is given in Eq. (25) and Eq. (26):

$$B_{rq}(\theta,t)=B_{rq0}(\theta,t)\cdot\lambda_{sr}(\theta,t), \tag{25}$$

$$B_{rq}(\theta,t)=\mu_0/g\times \left\{\begin{array}{l}\sum_u^{\infty}\sum_i^{\infty}K_{ui}\lambda_{s0}\lambda_{r0}\cos\left(u\theta\pm i\omega N_r t\right)+\\ \sum_u^{\infty}\sum_i^{\infty}\sum_n^{\infty}\frac{1}{2}K_{ui}\lambda_{s0}\lambda_{rn}\cos\left(\begin{array}{l}\left(u\pm nN_r\right)\theta\pm\\ \left(i\mp n\right)\omega N_r t\end{array}\right)+\\ \sum_u^{\infty}\sum_i^{\infty}\sum_m^{\infty}\frac{1}{2}K_{ui}\lambda_{r0}\lambda_{sm}\cos\left(\left(u\pm mN_s\right)\theta\pm i\omega N_r t\right)+\\ \sum_u^{\infty}\sum_i^{\infty}\sum_m^{\infty}\sum_n^{\infty}\frac{1}{2}K_{ui}\lambda_{sm}\lambda_{rn}\cos\left(\begin{array}{l}\left(u\pm\left(mN_s\pm nN_r\right)\right)\theta\pm\\ \left(i\mp n\right)\omega N_r t\end{array}\right)\end{array}\right\}. \quad (26)$$

Because three-phase 6/4 SRM is selected in this paper, so $1\le q\le Q=3$. Therefore, the linear magnetic flux density in the air gap is superimposed by the three-phase windings, as shown in Eq. (27):

$$\begin{aligned}B_{r,linear}&=B_{r1}(\theta,t)+B_{r2}(\theta,t)+B_{r3}(\theta,t)\\&=\mu_0/g\cdot\left(F_1+F_2+F_3\right)\cdot\lambda_s\cdot\lambda_r.\end{aligned} \quad (27)$$

D. The algorithm of magnetic saturation

Based on the linear radial magnetic flux density obtained by Eq. (27), the magnetic saturation should be taken into account. In this paper, the distributed equivalent reluctance and dynamic permeability are used to solve the magnetic saturation. In the above linear model, the air gap reluctance was considered only. While the permeability of the stator and rotor core was considered infinite. So, the reluctance of the stator and rotor core was neglected. But the local magnetic saturation of SRM is serious, especially the stator and rotor poles under the excitation state.

The circle of motor is divided into n parts. The saturated magnetic field of a single part can be analyzed by the equivalent magnetic circuit, as shown in Fig. 4. The reluctance of one part is defined as R_m, which can be equivalent to the superposition of the air-gap reluctance R_2 and the stator and rotor core reluctance R_3 (defined as the series reluctance R_3). The local magnetic saturation of SRM is mainly in the front half of the stator and rotor poles, so the length l of the series reluctance R_3 is about half of the total length of stator and rotor poles, i.e., $(h_s+h_r)/2$. In addition, d_0 is the width of each equivalent reluctance in Fig. 4; g is the length of the air-gap reluctance; $h_s/2$ is the length of the stator core reluctance; $h_r/2$ is the length of the rotor core reluctance.

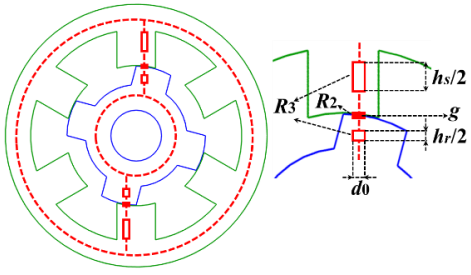

Fig. 4. The equivalent magnetic circuit.

The air gap reluctance R_2 and the series reluctance R_3 are shown in Eqs. (28) and (29). Where h is the effective length of the rotor core and μ_d is the dynamic permeability:

$$R_2=g/\left(\mu_0 d_0 h\right), \quad (28)$$

$$R_3=l/\left(\mu_d d_0 h\right). \quad (29)$$

Then, the equivalent reluctance R_m can be gotten by Eq. (30):

$$R_m=R_2+R_3. \quad (30)$$

Besides, the magnetic flux and the magnetic flux density are calculated by Eqs. (31) and (32), respectively:

$$\phi=F/R_m, \quad (31)$$

$$B_r=\phi/\left(d_0 h\right). \quad (32)$$

Substituting Eqs. (28)-(31) into Eq. (32), the saturated magnetic flux density can be gotten, as shown in Eq. (33), where the MMFs can be obtained by Eq. (15):

$$B_{r,saturation}=\left(F_1+F_2+F_3\right)\cdot\lambda_s\cdot\lambda_r/\left(g/\mu_0+l/\mu_d\right). \quad (33)$$

In Eq. (33), only the value of dynamic permeability μ_d is required. The μ_d is obtained by $\mu_d=B/H$ from the $B(H)$ curve, to draw the $\mu_d(B)$ curve, which is shown in Fig. 5.

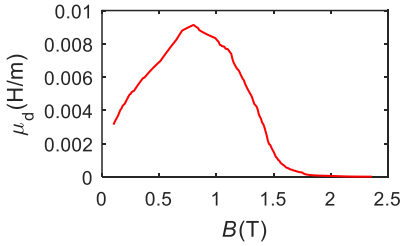

Fig. 5. The μ_d(B) curve.

Based on Eq. (33), combined with the $\mu_d(B)$ curve in Fig. 5 and the algorithm of magnetic saturation in Fig. 6, the dynamic permeability μ_d in the spatial circle at different rotor position can be captured. Therefore, the saturated magnetic density can be obtained. The radial magnetic flux density obtained by Method II in the three-phase 6/4 SRM is presented in Fig. 7, from which the radial magnetic density in the saturated region with Method II has a good agreement with the FEM. However, there is an enormous error between the analytical result and the FEM in the linear region, mainly because Method II can only calculate the radial magnetic flux density, neglecting the tangential magnetic flux density.

From the above, the radial magnetic density in the saturated region is accurate with Method II, which can be used to solve the magnetic saturation of SRM. However, the limitation of Method II is that the contribution of tangential magnetic density cannot be taken into account, which results in a significant deviation between the analytical result and the FEM in

the linear region. To obtain the saturated radial and tangential flux density, this paper presents a synthetic method based on Method I and Method II.

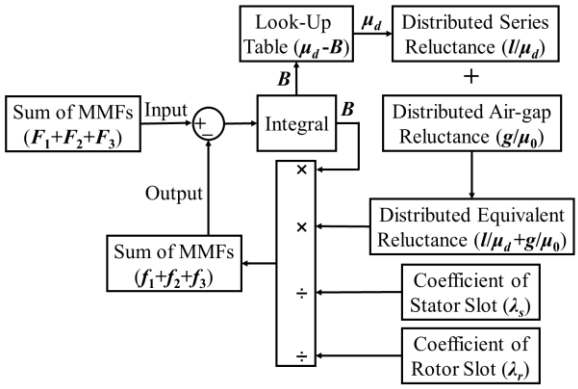

Fig. 6. The algorithm of magnetic saturation.

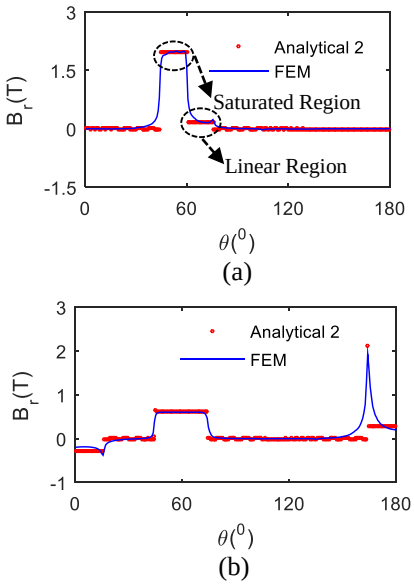

Fig. 7. The radial magnetic flux density: (a) unaligned position, and (b) aligned position.

V. THE SYNTHETIC METHOD

The main thinking of the synthetic method is shown as follows. The advantages of Method I and Method II are applied comprehensively. Because the tangential magnetic flux density which is mildly saturated is much less than the radial magnetic flux density, so Method I can be applied to predict the tangential magnetic flux density. Also, it can be seen from Fig. 5 that the magnetic over 1.5 T is severely saturated. So, for the radial magnetic flux density, it is calculated by Method I in the mildly saturated and linear region below 1.5 T; it is computed by Method II in the severely saturated region over 1.5 T. Therefore, the magnetic flux density considering the saturation in the air gap can be gotten by the synthetic method.

A. The magnetic flux density verification

The air-gap magnetic flux densities obtained by the synthetic method at the unaligned and aligned position in the three-phase 6/4 SRM are shown in Fig. 8 and Fig. 9, respectively. It can be seen from Fig. 8 and Fig. 9 that the analytical result is in good agreement with the FEM and the error is within 5%, indicating that the synthetic method is working.

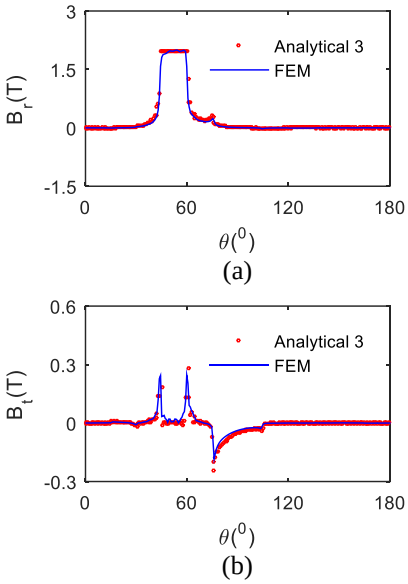

Fig. 8. The magnetic flux density at the unaligned position: (a) radial and (b) tangential.

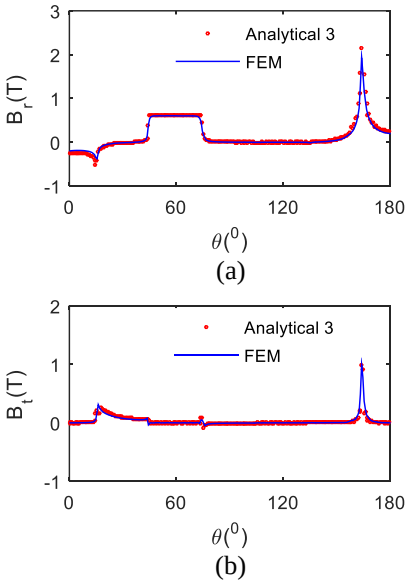

Fig. 9. The magnetic flux density at the aligned position: (a) radial and (b) tangential.

B. The radial electromagnetic force and torque verification

To further verify the above synthetic method, the radial electromagnetic force and torque are obtained by Maxwell Stress equation, which is compared with the FEM. The radial electromagnetic force at different rotor position is given in Fig. 10. Besides, the torque is presented in Fig. 11. Whether the electromagnetic force or the torque, the analytical results agree well with the FEM and the error is within 10%, which further indicates the accuracy of the synthetic method.

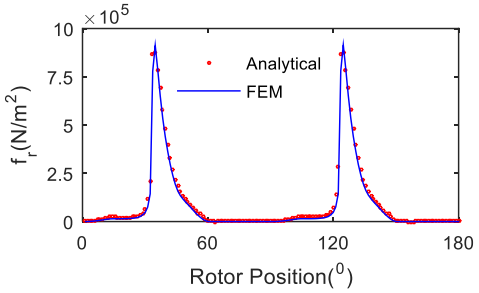

Fig. 10. The radial electromagnetic force at different rotor position.

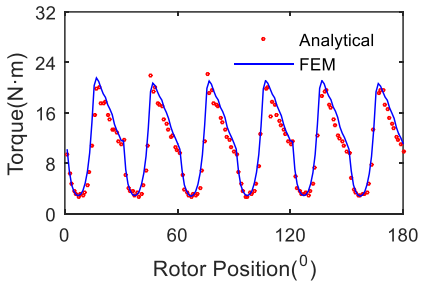

Fig. 11. The torque at different rotor position.

The computational time for the magnetic flux density calculation in all three-phase 6/4 SRMs in the aligned and unaligned position is given in Table 2. It can show in Table 2 that the speed of analytical computation is about twice that of finite element calculation. Therefore, the synthetic analytical method is much more time-efficient.

Table 2: Computational time

Rotor Position	Analytical /s	FEM /s
Aligned	3.95	8.09
Unaligned	3.67	7.56

VI. CONCLUSION

Although the finite element method always works well, it requires a huge amount of time and computational resources. By contrast, the analytical method is much more time-efficient and cost-effective. Therefore, it is worthwhile to investigate the analytical method for calculating the magnetic field of SRM. Moreover, the proposed synthetic analytical method can be applied to analyze quickly the effect of structural and electromagnetic parameters on the magnetic field of motor. Besides, the proposed method can be used together with the torque and vibroacoustic calculation method to optimize motors' torque ripple and electromagnetic noise, which can improve the design of motor. Besides, Method I is only applicable to the mildly saturated magnetic field, in which the maximum magnetic flux density is below 1.5 T. Also, Method II can precisely predict the severely saturated magnetic field, but the tangential magnetic flux density is not taken into account. Finally, the synthetic method based on the advantages of Method I and Method II can predict the air-gap magnetic field in SRM with accuracy. Besides, the maximum relative error between the magnetic flux density obtained by the synthetic method and that by FEM is not more than 5%. In addition, the radial electromagnetic force and torque are compared with the FEM, verifying the effectiveness of the synthetic method. It lays the foundation for the optimization of torque ripple, vibration and noise of SRM.

ACKNOWLEDGMENT

This work was supported by a Grant (Project 51875410) from the National Natural Science Foundation of China.

REFERENCES

[1] X. Liang, G. Li, J. Ojeda, M. Gabsi, and Z. Ren, "Comparative study of classical and mutually coupled switched reluctance motors using multiphysics finite-element modeling," *IEEE Trans. Ind. Electron.*, vol. 61, no. 9, pp. 5066-5074, Sep. 2014.

[2] H. Torkaman, N. Arbab, H. Karim, and E. Afjei, "Fundamental and magnetic force analysis of an external rotor switched reluctance motor," *Applied Computational Electromagnetics Society Journal*, vol. 26, no. 10, pp. 868-875, Oct. 2011.

[3] H. Cheng, H. Chen, and Z. Yang, "Design indicators and structure optimisation of switched reluctance machine for electric vehicles," *IET Electr. Power Appl.*, vol. 9, no. 4, pp. 319-331, Apr. 2015.

[4] T. Miller, "Optimal design of switched reluctance motors," *IEEE Trans. Ind. Electron.*, vol. 49, no. 1, pp. 15-27, Feb. 2002.

[5] S. Corovic, R. Benedetic, and D. Miljavec, "Modal analysis of different stator configurations to mitigate electromagnetically excited audible noise and vibrations of switched reluctance motors," *Applied Computational Electromagnetics Society Journal*, vol. 32, no. 12, pp. 1089-1097, Dec. 2017.

[6] L. Chen and W. Hofmann, "Speed regulation

technique of one bearingless 8/6 switched reluctance motor with simpler single winding structure," *IEEE Trans. Ind. Electron.*, vol. 59, no. 6, pp. 2592-2600, June 2012.

[7] X. Wang, Q. Li, S. Wang, and Q. Li, "Analytical calculation of air-cap magnetic field distribution and instantaneous characteristics of brushless dc motors," *IEEE Trans. Energy Convers.*, vol. 18, no. 3, pp. 424-432, Sep. 2003.

[8] Z. Zhu, D. Howe, and C. Chan, "Improved analytical model for predicting the magnetic field distribution in brushless permanent-magnet machines," *IEEE Trans. Magn.*, vol. 38, no. 1, pp. 229-238, Jan. 2002.

[9] Z. Zhu and D. Howe, "Instantaneous magnetic field distribution in brushless permanent magnet DC Motors, Part II: Armature-reaction field," *IEEE Trans. Magn.*, vol. 29, no. 1, pp. 136-142, Jan. 1993.

[10] K. Boughrara, T. Lubin, and R. Ibtiouen, "General subdomain model for predicting magnetic field in internal and external rotor multiphase flux-switching machines topologies," *IEEE Trans. Magn.*, vol. 49, no. 10, pp. 5310-5325, Oct. 2013.

[11] S. Mendaci, H. Allag, and M. Mekideche, "Multi-objective optimal design of surface-mounted permanent magnet motor using NSGA-II," *Applied Computational Electromagnetics Society Journal*, vol. 32, no. 5, pp. 519-526, May 2015.

[12] Y. Zhang, S. Ho, H. Wong, and G. Xie, "Analytical prediction of armature-reaction field in disc-type permanent magnet generators," *IEEE Trans. Energy Convers.*, vol. 14, no. 4, pp. 1385-1390, Dec. 1999.

[13] R. Sprangers, J. Paulides, B. Gysen, and E. Lomonova, "Magnetic saturation in semi-analytical harmonic modeling for electric machine analysis," *IEEE Trans. Magn.*, vol. 52, no. 2, Feb. 2016.

[14] R. Sprangers, J. Paulides, K. Boynov, E. Lomonova, and J. Waarma, "Comparison of two anisotropic layer models applied to induction motors," *IEEE Trans. Ind. Appl.*, vol. 50, no. 4, pp. 2533-2543, July-Aug. 2014.

[15] Z. Djelloul-Khedda, K. Boughrara, F. Dubas, and R. Lbtiouen, "Nonlinear analytical prediction of magnetic field and electromagnetic performances in switched reluctance machines," *IEEE Trans. Magn.*, vol. 53, no. 7, July 2017.

[16] H. Chen, D. Li, R. Qu, Z. Zhu, and J. Li, "An improved analytical model for inductance calculation of interior permanent magnet machines," *IEEE Trans. Magn.*, vol. 50, no. 6, June 2014.

[17] Q. Li, T. Fan, and X. Wen, "Armature-reaction magnetic field analysis for interior permanent magnet motor based on winding function theory," *IEEE Trans. Magn.*, vol. 49, no. 3, pp. 1193-1201, Mar. 2013.

[18] G. Dajaku and D. Gerling, "Stator slotting effect on the magnetic field distribution of salient pole synchronous permanent-magnet machines," *IEEE Trans. Magn.*, vol. 46, no. 9, pp. 3676-3683, Sep. 2010.

[19] B. Gaussens, E. Hoang, O. de la Barriere, J. Saint-Michel, P. Manfe, M. Lecrivain, and M. Gabsi, "Analytical armature reaction field prediction in field-excited flux-switching machines using an exact relative permeance function," *IEEE Trans. Magn.*, vol. 49, no. 1, pp. 628-641, Jan. 2013.

[20] M. Farshadnia, M. Cheema, R. Dutta, and J. Fletcher, "Analytical modeling of armature reaction air-gap flux density considering the non-homogeneously saturated rotor in a fractional-slot concentrated-wound IPM machine," *IEEE Trans. Magn.*, vol. 53, no. 2, Feb. 2017.

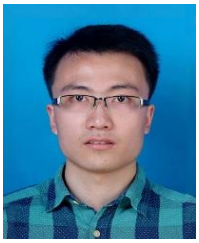

Shenglong Hu a Ph.D. candidate majoring in Vehicle Engineering at Tongji University, Shanghai, China. He received the Bachelor degree of Vehicle Engineering in 2016 from Dalian University of Technology, Dalian, China. His main research interests are in the control of vibration and noise of motor.

Shuguang Zuo a Professor at Tongji University, Shanghai, China. He received the B.S. degree in Mechanical Design from Hunan Agricultural University, Changsha, China, in 1990, and the M.S. and Ph.D. degrees in Automotive Engineering from Jilin University, Changchun, China, in 1993 and 1996, respectively. From 1996 to 1998, he was a Postdoctoral Researcher with the Aviation and Aerospace Technology Postdoctoral Research Station, Nanjing Aeronautics and Astronautics University, Nanjing, China. He is now a Professor with the College of Automotive Engineering, Tongji University. His research interests include vehicle system dynamics and control, vehicle vibration and noise control, and vibration and noise of electrical machines.